Understanding the physical determinants of pressure denaturation: Temperature switches the pressure-induced unfolding pathway

Christian Roumestand[1]*, Erika Dudas[2], Rita Puglisi[3], Antonino Calió[2], Philippe Barthe[1], Piero Andrea Temussi[4], Annalisa Pastore[5]*

[1]Centre de Biochimie Structurale, CNRS UMR 5048, University of Montpellier-INSERM U 1054, 29 Rue de Navacelles, 34090 Montpellier, France

[2]European Synchrotron Radiation Facility, Ave des Martyrs, 38000 Grenoble, France

[3]GSK Vaccines, Siena, Italy

[4]Department of Chemistry, Universita' Federico II, Napoli, Italy

[5]The Wohl Institute, King's College London, 5 Cutcombe Rd, London SE59RT, UK

[6]Elettra Sincrotrone Trieste, Strada Statale 14 - km 163,5 in AREA Science Park 34149 Basovizza, Trieste, Italy

*****To whom correspondance should be addressed

Running title: High-pressure NMR studies of Yfh1

Keywords: frataxin; high-pressure nuclear magnetic resonance; thermodynamic stability; protein folding; Yfh1

Abstract

Proteins unfold under different environmental insults, among which heat, cold, high pressure and chaotropic agents. Understanding the mechanisms that determine unfolding under each of these condition is an important problem that directly relates to the physical forces that determine the three-dimensional structure of a protein. Here, we studied the mechanism of pressure unfolding of the marginally stable yeast protein Yfh1 using high-pressure nuclear magnetic resonance as this is the most appropriate technique to obtain a residue-specific description of the folding/unfolding transitions of a protein. We demonstrate that the pressure-unfolded spectrum shares features in common with that at low but not at high temperature and room pressure, suggesting a tighter similarity between the two processes that could be explained by a similar role of hydration in the process. This is the first time that comparison between the three infolded states could be tested experimentally, and confirms something that up to now has been only suggested as an hypothesis. By recording the phase diagram of the protein, we also show that temperature switches the pressure-induced unfolding pathway suggesting a synergic mechanism between pressure- and temperature-induced denaturation: at moderate pressures, Yfh1 unfolding at low temperature starts at a patch of negatively charged residues that we have previously demonstrated to induce electrostatic frustration and cause cold denaturation. Heat unfolding involves instead a cavity created by insufficient protection of the hydrophobic core. These observations help us to reconstruct the structural events determining unfolding and distinguish the mechanisms that rule the different processes of unfolding.

Introduction

The study of protein unfolding, which corresponds to the process of loss of tertiary structure acquired after the amino acid chain has come out from the ribosome, has fascinated and keeps fascinating generations of scientists because its elucidation holds the promise of understanding the forces that determine protein structure formation. However, structure may be lost, both *in vivo* and *in vitro*, in several different ways, so that speaking about a unique unfolded structure is thus utterly meaningless (Pastore and Temussi, 2022). In nature, unfolding can be triggered by loss/gain of post-translational modifications, mutations, or any imbalance in the environmental conditions (*e.g.* changes in pH, protein concentration, crowding, confinement, etc.). *In vitro*, unfolding can be triggered by changes in temperature, pH, solvent composition, and/or pressure. Among these causes, pressure-induced denaturation is probably the process relatively less studied, possibly because of the non-trivial experimental problems posed by pressurization. The process remains nevertheless extremely interesting both because some proteins do experience unusually high pressure in nature (*e.g.* proteins from organisms that live in the deep seas) and because it may involve atomic forces probably less dominant in other unfolding processes but not for this less important. These considerations call for a more attentive and detailed study of the mechanisms involved in pressure-induced unfolding.

Several aspects of pressure-induced unfolding remain unclear. Most studies of protein unfolding caused by pressure show, for instance, that it is necessary to reach high values of pressure (of the order of thousands of bars) before unfolding can be observed in common piezo-tolerant or pressure mesophile organisms. This might be considered at variance with the devastating effects that comparatively less drastic temperature increases may induce in proteins from common thermally mesophile organisms. It is also important to understand what happens during the long lag phases (between 1 and up to several kbar) that are observed in many of the pressure-induced unfolding processes.

We have recently studied the pressure unfolding of a marginally stable protein, Yfh1 from *S. cerevisiae*, that unfolds at pressures so low that its unfolding does not present the typical lag phase usually observed before a protein loses its fold (Puglisi et al., 2022). Yfh1 is a small protein (123 residues in its mature, full-length form) under several aspects remarkable: when depleted of salt, it is possible to observe its cold denaturation at temperatures above water freezing in solutions under quasi-physiological conditions (278 K or 5°C) (Pastore et al., 2007). The high temperature unfolding is also relatively low (around 308 K or 35°C). Also at room temperature, Yfh1 is in an equilibrium between folded and

unfolded forms, with a population of the unfolded form around 30%. Addition of even small quantities of salts causes disappearance of the unfolded form (Vilanova et al., 2014). The Yfh1 fold consists of two N- and C-terminal helices that pack on the same side against a 5-7 strand β-sheet depending on the species (Musco et al., 2000). Two interesting features were demonstrated to play an important role in Yfh1 stability. First, the C-terminus of Yfh1 is shorter as compared to other orthologues (*e.g.* it is three residues shorter than the bacterial orthologue and twelve residues shorter as compared to the human protein) (Adinolfi et al., 2004). When present, this secondary structure element inserts in between the two terminal helices protecting the hydrophobic core. Accordingly, the melting heat-induced temperatures at low salt of the yeast, bacterial and human proteins go from 308 K, to 328 K, up to 338 K (35°C, 55°C, 65°C) respectively, correlating with the C-terminus length. In Yfh1, where the extension is absent, the core is more easily accessible. In fact, we have demonstrated that shortening the human protein causes a major destabilization, whereas lengthening the yeast protein leads to stabilization (Adinolfi et al., 2004). A second feature is that Yfh1, but not other orthologues, contains four negative residues on the first and second strands (Sanfelice et al., 2014). This quadrilateral causes significant electrostatic frustration which ultimately leads to cold denaturation: mutation of only one of these residues to a neutral hydrophilic group leads to the shift of cold denaturation at temperatures below the water freezing point while not altering the high-temperature melting point. Having a system of which we understand in detail the elements that determine protein stability makes Yfh1 a precious tool which we have extensively exploited to probe the mechanisms that determine protein unfolding.

In a previous study, we determined the phase diagram of Yfh1 unfolding as a function of pressure (1-5000 bar) and temperature 278-313 K (5-40°C), both in the absence and in the presence of fold stabilizers using the intrinsic fluorescence of the two tryptophan residues of Yfh1 (Puglisi et al., 2022). Under these mild conditions, we demonstrated that Yfh1 has a remarkable sensitivity to pressure: 50% unfolding occurs already at pressures around 100 bar at room temperature. For comparison, more thermodynamically stable globular proteins, such as the immunoglobulin-like module of titin I27 or a hyper-stable variant of Staphylococcus nuclease, need pressures as high as 2-3 kbar to unfold in mild concentrations of guanidinium chloride, showing an incredible resilience (Herrada et al. 2018; Roche et al., 2012).

In the present study, we exploited these unusual properties for observing the thermodynamic parameters of Yfh1 at pressures above ambient pressure by nuclear magnetic resonance (NMR). This technique is almost unique in providing residue-specific information on the folding/unfolding pathway of a given protein (Pastore and Temussi, 2023; Roche et

al., 2017). We carried out a detailed study by recording the one- and two-dimensional HSQC spectra of the protein in the range 278-303 K and 1-1000 bar. We show that the pressure-unfolded spectrum shares features with the low but not the high temperature-unfolded spectrum, suggesting a similar mechanism. We also determined the phase diagram of the protein and, thanks to the residue-specific information provided by high-pressure NMR, we could reconstruct the early events that determine unfolding and show that, at all pressures, they involve the negatively charged patch previously identified as key in causing cold denaturation at low but not at high temperature (Sanfelice et al., 2014). This evidence provides us with a detailed model of how unfolding occurs under different conditions. We thus conclude that, as compared to fluorescence, NMR provides complementary information and allows a more thorough understanding of the processes occurring during protein unfolding.

Materials and Methods

Sample Preparation

The recombinant Yfh1 protein was produced as previously described (Adinolfi et al, 2002). In short, the ^{15}N-labeled protein was expressed in *Escherichia coli* BL21-(DE3) cells grown at 314 K (37 °C) in minimal medium using ammonium sulphate as the sole source of nitrogen, and induced by addition of 0.5 mM IPTG for 2 h. After cell harvesting by centrifugation, the cells were re-suspended in Tris-HCl buffer containing a complete EDTA protease inhibitor cocktail tablet (Roche) and lysed by sonication. The soluble protein was purified by two ammonium sulphate precipitation steps at 40% cut to precipitate contaminating proteins and a 65% cut to precipitate Yfh1. The protein was dialysed and further purified by anion exchange chromatography using a Pharmacia Q-Sepharose column with a gradient from 0 to 1 M NaCl, followed by a Pharmacia phenyl-Sepharose column with a decreasing 1 M ammonium sulphate gradient. The final samples were dialysed in 20 mM HEPES at pH 7.0. No additional salt was added since we had previously demonstrated that even small quantities of salt appreciably stabilize the protein (Adinolfi et al., 2004; Vilanova et al., 2014).

Protein unfolding monitored by high-pressure NMR Spectroscopy

A protein sample with about 0.5 mM concentration of ^{15}N-labeled Yfh1 in 20 mM HEPES at pH 7.0, with 2 mM DTT and containing 5% (v/v) D_2O for the lock, was used on a 5/3 mm O.D./I.D. ceramic tube (330 µl of sample volume) from Daedalus Innovations (Aston, PA,

USA). Hydrostatic pressure was applied to the sample directly within the magnet using the Xtreme Syringe Pump also from Daedalus Innovations. Two-dimensional [^{1}H,^{15}N] HSQC spectra were recorded on a Bruker AVANCE III 600 MHz spectrometer (standard ^{1}H-^{15}N double-resonance BBI probe), in the range 278-303 K, although in the end we used for the analysis only those at 283-303 K. At each temperature, the pressure was varied from 1 bar to 1000 bar by steps of 50 bar. Each pressure step lasted 2 h, starting with 1 h relaxation time, to allow the folding/unfolding reaction to reach full equilibrium, followed by a 1D spectrum (32 scans with 10 s of relaxation time, to ensure the complete relaxation of the methyl protons between each scan) and a 2D [^{1}H,^{15}N] HSQC (8 scans for each of the 128 complex points in the indirect dimension). The relaxation time preceding the recording of the 1D and 2D experiments was estimated from a series of one-dimensional NMR experiments recorded after a 300 bar P-Jump, following the exponential growth of the resonance band corresponding to the methyl groups in the unfolded state of the protein [Dubois et al, 2020]. Reversibility of unfolding was checked by comparing 1D and 2D [^{1}H,^{15}N] HSQC spectra recorded at the end of the series of experiments, after returning at 1 bar, with the experiments recorded at 1 bar before pressurization.

^{1}H chemical shifts were directly referenced to the methyl resonance of DSS (2,2-Dimethyl-2-silapentane-5-sulfonate, sodium salt), while ^{15}N chemical shifts were referenced indirectly to the absolute frequency ratios ^{15}N/^{1}H = 0.101329118. Water signal was suppressed by the WATERGATE pulse sequence (Piotto et al., 1992). The assignment of the amide resonances of Yfh1 was retrieved from the BioMagResBank (http://www.bmrb.wisc.edu, entry number 19991). Data processing and analysis were performed using GIFA (Pons et al., 1996). At each temperature, the cross-peak intensities for the folded species were measured at each pressure and then fit with a two-state model according to the equation:

$$I = \frac{I_{max} + I_{min} e^{-(\Delta G_u^0 + p\Delta V_u^0)/RT}}{1 + e^{-(\Delta G_u^0 + p\Delta V_u^0)/RT}} \qquad (1)$$

where I is the cross-peak intensity measured at a given pressure, and I_{max} and I_{min} correspond to the cross-peak intensities in the spectra of the folded protein at 1 bar and at 1000 bar, respectively. ΔG_u^0 stands for the variation of the residue-specific apparent free energy between the unfolded and the folded states at atmospheric pressure. ΔV_u^0 is the difference of the residue-specific apparent volume of the unfolded and the folded states during pressure

denaturation. In the fitting, I_{max}, I_{min}, ΔG_u^0 and ΔV_u^0 values were left as floating parameters. Once the ΔG_u^0 and ΔV_u^0 values were obtained, the residue-specific curves were normalized (I_{max}= 1 and I_{min} = 0 in Eq. 1) to the native fraction of the protein as a function of pressure.

Calculation of the thermodynamic parameters

Assuming that the difference in heat capacity, ΔC_p, between native and unfolded state is temperature independent, ΔG at constant pressure depends on temperature as described by the modified Gibbs-Helmhotz equation:

$$\Delta G = \Delta H_m \left[1 - \frac{T}{T_m}\right] + \Delta C_p \left\{(T - T_m) - T ln \left[\frac{T}{T_m}\right]\right\} \qquad (2)$$

where T_m is the temperature at the midpoint of the unfolding transition, and ΔH_m is the unfolding enthalpy change at T_m. The curve corresponding to this equation is known as the stability curve of the protein. The thermodynamic parameters were obtained by fitting this equation.

Calculation of the contact maps

Contact maps of the Yfh1 native structure, i.e. the matrix of contacts below a chosen threshold between residue i and j along the whole sequence, were obtained using the web-server CMView contact map (Vehlow et al., 2011; website: http://www.bioinformatics.org/cmview/) with a threshold of 8.5 Å around the C_α of each residue, using the best score AlphaFold model (Jumper, 2021) obtained by version 2.2 AlphaFold locally installed at the Centre de Biologie Structurale (University of Montpellier/CNRS/INSERM).

Results

Modelling a reference 3D structure of Yfh1

Although the structures of several Yfh1 orthologues from different species have now been solved, the structure of the yeast protein remains determined only at low resolution. Of the seven entries available in PDB, 2GA5 is an NMR structure which however has serious distortions of the geometry caused by assignment misinterpretation: as previously demonstrated (Vilanova et al., 2014), the authors mistraced the sequential assignment mixing resonances from the folded and the unfolded states. This caused strain and a poor geometry.

The other six structures, solved by crystallography at *ca.* 3 Å resolution, are those of a mutant in which a well conserved tyrosine (Tyr73) was substituted by an alanine (Söderberg et al., 2011). This mutation enhances the tendency of the protein to form large aggregates in the presence of high concentrations of iron but affects the structure of the N-terminal helix. The NMR and crystallographic structures superpose with a 2.5 Å rmsd (on residues 75 to 172 using the numbering of the mature protein and of the 3OEQ entry), with maximal differences in the orientation of the C-terminal helix and in the structure of the 6th and 7th putative ß-strands. To clarify the issue, we used AlphaFold to generate a model that could be consistent with the structures of all Yfh1 orthologues. The AlphaFold vs 2.2 software used for modelling yielded a model with a high degree of confidence: only eight out of the 123 residues of Yfh1 had a pLDDT (predicted local distance difference test) score lower than 0.9, all located at the N-terminal extremity of the molecule, which has been demonstrated to be intrinsically disordered and flexible (Popovic et al., 2015). (**Figure 1**). This model superposes with the crystal structure with a 1.1 Å rmsd in the globular region (residues 75-172), as compared to a 2.2 Å rmsd with the NMR structure. However, although a better superposition is observed for the ß-sheet between the X-ray structure (3OEQ) and the AlphaFold model, the lengths of the ß-strands are not always the same. The X-Ray structure also lacks the first two helical turns of the N-terminal helix (L70-E76) that are present both in the AlphaFold model and in the NMR structure (2GA5), due to the structural distortions induced by the Tyr73Ala mutation. The crystal structure lacks the two last residues (S172, Q173), yielding to a shortening of the C-terminal helix where an additional turn is observed both in the NMR structure and on the AlphaFold model. For these reasons, we decided to consider the AlphaFold model as the reference for any further analysis.

Yfh1 undergoes pressure denaturation under modest pressures

To explore the phase diagram of Yfh1, we recorded 1D ^{1}H and 2D [^{1}H,^{15}N] HSQC spectra in the pressure range of 1-1000 bar and between 283 and 303 K with a 5 K interval to analyse Yfh1 pressure unfolding at the residue level (Roche et al., 2017; Roche et al., 2019; Dubois et al., 2020). This range of pressure was chosen because previous high-pressure fluorescence spectroscopy studies of Yfh1 had demonstrated that the protein has the midpoint of unfolding between 100-200 bar (Puglisi et al., 2022). We compared the behaviour of the 1D peak areas versus temperature at atmospheric pressure with previous similar plots to assess reproducibility (Pastore et al., 2007), and observed an excellent agreement (**Figure S1**).

The 2D [^{1}H,^{15}N] HSQC spectra at 1 bar, all recorded temperatures and low ionic strength were of excellent quality, with high resonance dispersion and several high- and low-frequency resonances which demonstrated that the protein is mainly folded in the range of temperatures 283-303 K (**Figure 2**). The concurrent presence of the equilibrium between folded and unfolded species in the slow regime in the NMR timescale is evident from the co-existence in the HSQC spectra of well dispersed resonances in co-presence with a number of other peaks that change their intensity at different temperatures that are diagnostic of the unfolded species. An example is the cross-peak at 10 ppm/129 ppm (^{1}H/^{15}N). These resonances disappear upon addition of also minute concentrations of salt (Vilanova et al., 2014).

As usually observed, spectra at increasing pressures showed progressive attenuation of the resonances from the folded species (**Figure 2**). Conversely, the resonances of the unfolded species became increasingly intense and new peaks originally less intense or masked by other more intense resonances appeared. This behavior is consistent with a two-states equilibrium between the folded and unfolded states in the slow exchange regime in the NMR timescale, as well as with a two-state transition between each folded/unfolded pairwise cross-peak during the unfolding process. A total of 67 resonances (corresponding to 59% of the 114 non-proline residues) had no overlap with other peaks at any of the five temperatures and displayed cross-peaks of sufficient intensity at atmospheric pressure to be accurately fit by a two-state unfolding model, providing an appreciable number of local probes for the description of Yfh1 unfolding.

Above ca. 400 bar, we observed nearly complete disappearance of the well-dispersed species, suggesting almost complete unfolding of the protein. Some residual structure remained visible also at 600 bar at the noise level, but the relative ratio accounts for less than 2% of the initial intensity. The high-pressure spectra of the pressure-unfolded species at all recorded temperatures exhibited a similar collapse of the resonances, indicating that the primary denaturing agent is pressure (**Figure 2**).

After reaching 1000 bar, the sample was returned to 1 bar in two steps (500 and 1 bar). The spectra collected before and after pressurization were superimposable within 10% differences, demonstrating the almost complete reversibility of the process. This observation is fully in line with our previous experience with Yfh1, that is a protein altogether with relatively low tendency to aggregate (covalently and non-covalently).

Cold and pressure but not heat unfolding are tightly linked to the role of hydration

In previous studies, we had made a detailed comparison between the chemical shifts of the amide protons of the unfolded states at low and high temperatures (Adrover et al., 2010 and 2012). We had found that the amide secondary chemical shifts, that is the difference between the experimental values from a given residue and the random-coil values recorded at 298 K for model tetrapeptides (Wishart et al., 1995), had consistent different and opposite signs: the values measured at low temperature were negative, implying deshielding, whereas those at high temperature were positive, indicating shielding effects (Adrover et al., 2010). We had explained these results by a different degree of hydrogen bonding of the amides with water, reflecting a higher degree of hydration at low temperature.

Here, we compared the spectra of the unfolded states at 15°C, where the protein reaches its maximum of stability, and at high pressure (800 bar) with those obtained at high and low temperature and atmospheric pressure (Adrover et al., 2010) (**Figure 3**). Several observations could be extracted from the comparison: first, a similar level of collapse of the spectrum is evident in all three conditions, indicating population of mostly unfolded states. Second, the appearance of the spectrum at high pressure is overall closer to that at low temperature and 1 bar, while the high temperature spectrum appeared more broadened, likely indicating a higher degree of conformational exchange between species. Third, the spectrum at high pressure exhibits an overall low-field shift which suggests deshielding similar to that at low temperature and 1 bar. This can be seen by comparing the overall position of the spectra as compared to an ideal oval plot in the same position. The shift is also evident for the well-isolated resonances of the only two tryptophan residues in the sequence, one buried and one exposed that are visible around 10.2 ppm and 130 ppm in the proton and nitrogen dimensions respectively in all denatured spectra (**Figure 3**). Due to sequential effects, the two peaks are not completely superposable indicating residual local level of asymmetric environment, but they are clearly downfield shifted in the cold denatured and high-pressure spectra by ca. 0.2 ppm as compared to high temperature.

Altogether, these observations can be explained by a similar degree of hydrogen bonding strength of the amides with water at low temperature and high pressure, indicating a strong effect of hydration in the process and a higher similarity between these two unfolded states as compared to the high temperature one.

Evaluating the effect of pressure on ΔG_u^0 and ΔV_u^0

Fitting the cross-peak intensities with the corresponding two-state equation (Eq.1) provided residue-specific values for the apparent free energy (ΔG_u^0) of unfolding (**Figure 4**), which

reports on the protein stability, and the apparent volume change (ΔV_u^0) of unfolding (**Figure 5**), which corresponds to the volume difference between the folded and the unfolded states of the protein.

The two-state model was adequate to fit most of residue-specific unfolding curves, even though the absence of points describing the upper plateau (I_{max}) of the sigmoid, due to partial unfolding already at 1 bar, yielded significant error bars for the apparent residue-specific free energy values ΔG_u^0 and, to a lesser extent, for the residue-specific ΔV_u^0 values (**Figure 4 and 5**). This is especially true for experiments recorded at 303 K, temperature at which several residues exhibit negative values of ΔG_u^0, meaning that these residues are in an unfolded conformation at atmospheric pressure for more than half of the protein population.

Yfh1 displays low stability, that appears to be maximal around 288 K, with an average value for the apparent free energy of unfolding $<\Delta G_u^0>$ of 649 ± 145 cal/mol, and significantly decreases at higher and lower temperatures (**Table 1**). These values are remarkably low when compared to what usually observed for other small globular proteins, that often needed the presence of guanidinium chloride to observe pressure unfolding within a feasible pressure range (Roche et al., 2012; Herrada et al., 2018; Saotome et al., 2019, Lahfa et al., 2023). The dependence of $<\Delta G_u^0>$ on temperature exhibited a concave profile with a maximum around 288 K (**Figure 4**). Fitting the temperature dependence of $<\Delta G_u^0>$ to the Gibbs-Helmotz equation (Eq. 2) yielded the thermodynamic parameters ΔCp of unfolding (1 ± 0.7 kcal/mol.K), T_m (305 ± 4 K) and ΔH_m, (19 ± 7 kcal/mol) (**Figure 4**) in excellent agreement with previous studies (Pastore et al., 2007; Martin et al., 2008).

A linear decrease with temperature was observed for the average absolute values of the apparent ΔV_u^0 **(Figure 5)**. The slope of this dependence of ΔV_u^0 on temperature corresponds to the difference in thermal expansivity, Δα, between the folded and unfolded states of the protein. A value of Δα = 2.7 ± 0.7 ml/mol.K was estimated that is comparable to those found in the literature (Dubois et al., 2021; Fossat et al., 2016; Dellarole et al., 2015; Rouget et al., 2010). On the other hand, the absolute values found for ΔV_u^0 (≈ 150 ml/mol) are substantially greater than those usually found for proteins of comparable size and from those measured on Yfh1 by fluorescence spectroscopy (≈ 90 ml/mol) (Puglisi et al., 2022).

The residue-specific apparent values of ΔV_u^0 and ΔG_u^0 were used to build normalized residue-specific denaturation curves, giving the fraction of folded species for each residue as a function of pressure for each of the five temperatures used in this study (**Figure 6**). The average normalized curve was then calculated from the individual residue-specific normalized curves, giving information on the global evolution of the native fraction of the

protein during pressure unfolding. Plots of the evolution of the native fraction as a function of the temperature at different pressures (1, 150, 300, 450 and 600 bar) showed a maximum for the native fraction around 288 K (**Figures 6**), consistent with the temperature dependence of ΔG_u^0. Interestingly, the differences observed between temperatures diminish when increasing the pressure, until merely vanishing at high pressure (600 bar), indicating that the total unfolding of the protein is reached around the same pressure whatever the temperature. This strongly suggests that temperature does not only affect the stability of the protein, but also the cooperativity of unfolding.

The role of electrostatic frustration in cold denaturation at low temperature

As already reported for other proteins, it is possible to characterize the folding pathway of a protein by visualizing the regions of the protein that progressively become unfolded at increasing pressures following a procedure previously described (Roche et al., 2012; Roche et al., 2013). We defined the probability of contact for each pair of residues, $P_{i,j}$, as the geometric mean of the fractional probability of the two residues at a given pressure using the relation (Fossat et al., 2016):

$$P_{i,j} = \sqrt{P_i \times P_j}$$

where the fractional probability P_i or P_j correspond to the probability to find residue *i* or *j* in the native state at a given pressure for a given temperature. These fractional probabilities are obtained directly from the normalized residue-specific denaturation curves obtained for each residue (Dubois et al., 2020).

Using CMview **(**Vehlow et et., 2011) with a generous cut-off distance threshold of 9.5 Å, a total of 662 (non-sequential) contacts between the Cα of the 123 residues of the protein could be measured from the AlphaFold model of Yfh1. Of them, 250 contacts concern the 67 residues for which residue-specific denaturation curves could be obtained. We then plotted the evolution of the corresponding $P_{i,j}$ probabilities as a function of pressure and temperature (**Figure S2**), assuming that a contact is "lost" when $P_{i,j} < 0.5$. Consistent with the ΔG_u^0 values, the number of lost contacts at 150 bar is much less important at 288 K than at lower or higher temperatures, reflecting the higher stability of the protein at this temperature. Virtually all the contacts were lost at 200 bar at all temperatures, with partial unfolding of the protein starting at 50 bar at 283 K, 293 K and 298 K. Note that at this pressure, the number of lost contacts is above 60% at 303 K, confirming that the protein is already severely denatured under these conditions. At 288 K, the unfolding transition appears more cooperative, with only 6% of lost

contacts at 125 bar, although the protein is almost totally unfolded at 200 bar. Thus, the higher stability of the protein at this temperature is associated with a higher cooperativity of its unfolding transition.

We then built fractional contact maps from the probabilities of contact calculated at the five temperatures (**Figure 7**). At 283 K, few long-range contacts are lost ($P_{i,j} < 0.5$) in the ß-sheet at 50 bar, as well as a few long-range contacts in the ß-sheet, as well as a few long-range contacts between the beginning of the ß-sheet and the N-terminal helix. It is noteworthy to remember that the negatively charged patch that has been identified to determine cold denaturation involves residues in the first two strands of the ß-sheet and the N-terminal helix (Sanfelice et al., 2014). At 100 bar, contact loss concerns more residues in the ß-sheet, and also to long-range contacts between the ß-sheet and the two helices. At this pressure, the N-terminal helix begins to unfold, whereas the C-terminal helix remains mostly unaffected. At 150 bar, almost all contacts are lost. At 288 K, that is close to the maximal stability temperature, unfolding appears very cooperative, starting only at 150 bar, and concerns all the secondary structure elements, as well as the tertiary contacts between them. At 200 bar, virtually all contacts are lost, confirming the higher cooperativity of the unfolding reaction at this temperature. At higher temperatures, contrary to what observed at 283 K, unfolding becomes again less cooperative, and contact loss concerns first the C-terminal helix (50 bar) and then extends to the ß-sheet (100 bar), the N-terminal helix being the last secondary structure element to unfold. At 303 K, almost all contacts are already lost at 50 bar, hampering comparison with the other temperatures.

As a conclusion, these results indicate that temperature does not only modify the onset and the cooperativity of the unfolding transition, but also affects the unfolding pathway. This important observation is in agreement with a different mechanism of unfolding for the high and low temperature and pressure transitions.

Discussion

Here, we report a study of the properties under pressure-induced unfolding of Yfh1, a small globular protein from yeast and a member of the frataxin family highly conserved from bacteria to primates (Castro et al., 2019). Yfh1 is a unique model system that, thanks to its marginal stability, is particularly suited to study the mechanisms of protein unfolding under different denaturing agents (Pastore and Temussi, 2023). Pressure denaturation studies are interesting because they allow us to reach an important part of the phase diagram of protein unfolding that could not be accessed otherwise. They can also, in principle, access unfolding

without the need of adding chaotropic agents such as urea or guanidinium that, inherently, perturb the chemical environment and changes the solvation state of proteins, acting as co-solvents (Pastore and Temussi, 2023).

In a previous study based on the intrinsic fluorescence of the two tryptophan residues present in the Yfh1 sequence, we had used pressure as a means of structural perturbation (Puglisi et al., 2022). We had shown that Yfh1 is a system exquisitely sensitive to pressure since the protein can be pressure-unfolded at values appreciably lower those required for unfolding most of the small globular proteins reported so far: it is needed to use pressures of circa 500-800 bar for the practically complete unfolding of Yfh1 *versus* the often >2000 bar needed for other proteins (Roche and Royer, 2018; Smeller, 2002). In the present study, we complemented our previous fluorescence-based investigations using NMR, since this technique is uniquely suited for protein unfolding studies at the residue-specific level, providing local information on the behaviour of different regions of a protein, as previously demonstrated for the unfolding of Yfh1 by temperature (Puglisi et al., 2021; Puglisi et al., 2020).

Our phase diagram covered the range of 1-1000 bar and 283-303 K, although we could comfortably go below and above these temperatures. We decided to restrict our analysis to temperatures at which this marginally unstable protein is not strongly destabilized at atmospheric pressure (Adinolfi et al., 2004), to be able to distinguish between the effects of pressure and temperature.

We observed a qualitatively similar pattern at all temperatures: according to our previous work (Puglisi et al., 2022), the unfolding pre-transition starts already at 50 bar. Around 400 bar, the molecule is almost completely unfolded with almost complete, but not total, with disappearance of the well-dispersed resonances from the folded species. Some residual peaks from the folded structure remain also at 600 bar as it can be observed through the retention of resonances from the folded species in the spectrum, but the relative ratio accounts for less than 2% of the initial intensity, which is close to the noise level (data not shown). It is worth mentioning that we had observed the same minor retention of the folded spectrum also in NMR spectra recorded at low and high temperatures and at atmospheric pressure at values at which the CD spectrum of the unfolded species had reached a plateau (Pastore et al., 2007; Adrover et al., 2012). This indicates once again that NMR is a technique uniquely sensitive to detect even minute residual quantities of a species, under conditions when other techniques could not compete.

It is interesting to compare the thermodynamics parameters obtained from fluorescence and NMR measurements. The ΔG and ΔV values obtained in our prior work using high-pressure fluorescence (Puglisi et al., 2022) (**Table 1**) are significantly smaller than those reported here from high-pressure NMR. The discrepancy between both the ΔG and ΔV values could be explained by remembering that the intrinsic Trp fluorescence reports on variations of the local environment of the Trp side chains, which does not necessarily coincide with the global transition of the protein structure. Additionally, fluorescence spectroscopy observed all the states of the protein: unfolded, folded and potential intermediate states, while, in our exchange regime, NMR reflects only the folded and unfolded states. Any multiple states populated during the unfolding, with possibly small ΔV, would be averaged in fluorescence resulting in ΔV values smaller than those measured by NMR. Accordingly, our fluorescence data seem to indicate at least a 3-states equilibrium (2 different slopes). Interesting to notice is also that the thermal expansivity, that is the slope of the ΔV as a function of the temperature, is 2.30 ml/mol°C for Yfh1, that is, albeit larger, in the order of magnitudes of values reported for proteins of similar size in other studies (1.15 ml/mol°C for GIPC10 (Dubois et al., 2021) and 1.71 ml/mol°C for pp32 (Fossat et al., 2016)).

Overall, there are several important and novel conclusions of the present study that give us a new perspective of the effect of pressure on protein unfolding and the role that hydration plays in it. First, our data collectively hint at a higher similarity between the mechanism that govern cold and pressure denaturation over high temperature: the overall clear-cut low-field chemical shifting of the spectrum under these two conditions as compared to the high temperature unfolded spectrum clearly speaks in favour of a de-shielding effect of the amide protons. While this conclusion has been suggested before, this is the first example in which experimental data clearly support this hypothesis. This observation suggests a similar role of hydration for the cold and pressure unfolding.

Second, our analysis allows us to follow the unfolding pathway at the residue level. Interestingly, we observed that temperature influences the pathway taken by the protein during pressure unfolding, that is the pattern of unfolding upon increasing pressure, clearly depends on the temperature. At 288 K, that is the temperature where the protein is close to its maximum of stability, the unfolding is cooperative, close to a global two-state equilibrium between the folded and unfolded populations of the protein. Out of this zone of stability, the unfolding mechanism becomes less cooperative, and a switch between different pathways can be observed depending on whether pressure unfolding occurs at low or at high temperature.

At low temperature (283 K), partial unfolding concerns primarily the first strands of the ß-sheet, as it has been already observed for cold denaturation (Bitonti et al., 2022; Sanfelice et al., 2014). At high temperature, unfolding concerns first the C-terminal helix and then extends to the ß-sheet. This behaviour suggests a synergic mechanism between pressure- and temperature-induced denaturation. It also implies a different mechanism of unfolding at high and low temperature according with Privalov's theory (1979, 1982, 1990) by which the cold denaturation is mostly under the enthalpic control and strongly depends on the higher affinity of water to apolar groups and on the hydrogen bonding with the solvent, while heat denaturation is entropically driven resulting from the increasing molecular motions. At higher pressures, unfolding is more cooperative indicating a sudden collapse of the structure and the opening of the hydrophobic core due to increased molecular motions.

We could say that, metaphorically speaking, it is as if there were two "doors" on the structure of the protein that promote unfolding, one for the cold temperature, the other for the hot one. At high temperature, the C-terminus and the cavity between the two helices created by the shorter C-terminus in Yfh1 become the predominant elements for disruption of the fold. Instead, the secondary structure elements that we observe to unfold first at low temperature, the N-terminal helix and the beginning of the β-sheet, contain the quadrilateral of negative charges that introduces electrostatic repulsion in the structure that is one of the two elements that induce cold denaturation (Bitonti et al., 2022; Sanfelice et al., 2014; Vilanova et al., 2014). Repulsion between these residues creates a strain that, under destabilizing conditions, favours opening of the three-dimensional structure and entrance of water in the hydrophobic core, determining unfolding. We have in fact observed before that mutation of a single residue from the negatively charged quadrilateral to a neutral one is sufficient to shift cold denaturation at temperature below the freezing point while leaving unchanged the high temperature transition (Sanfelice et al., 2015). Based on this evidence, we were also able to reconstruct the rules that induce cold denaturation and applied them to detect this transition in an otherwise stable orthologue of Yfh1 (Bitonti et al., 2022). Thus, the data presented here demonstrate unequivocally the importance of this charged patch on the stability of the protein and on the mechanism of cold denaturation.

Finally, it has been suggested that pressure denaturation depends on the elimination of the solvent-excluded internal voids and/or on the water penetration inside the core of the macromolecule. Accordingly, pressure denaturation studies provide an important thermodynamic parameter, that is the volume changes upon unfolding, ΔV. This parameter is defined as the difference between the system (o.e. the protein and the solvent) volumes of the

unfolded and the folded states (or viceversa reversing the sign). Over the range of temperature considered in the present study, we consistently found that pressure denaturation perturbs the folded state by reducing the volume of the unfolded state, leading to negative values of ΔV. The difference is persistently larger at lower temperatures but becomes smaller at higher temperatures, suggesting that increasing the temperature causes a more compact and less compressible state. The temperature-dependent decrease in the absolute value of ΔV_u^0 is a well-known effect that has been ascribed to the difference in thermal expansion between the folded and unfolded states (Roche and Royer, 2018). However, we observe a consistent decrease of the absolute value of ΔV_u^0 also at temperatures at which the protein is cold denatured (Puglisi et al., 2022). This means that the thermal expansion of all protein states arises from the fact that hydration contributes to the system volume more significantly at lower temperatures due to stronger hydrogen-bonding, whereas waters will be increasingly more dynamic at higher temperatures, thus resulting in a lower contribution.

In summary, our report describes the pressure unfolding of Yfh1 and allowed us to follow the unfolding pathway of the protein as a function of pressure and temperature in a residue-specific way. We could thus trace the regions of Yfh1 which unfold first and determine a model that could explain the mechanism of unfolding. The two main conclusions of our study are the higher similarity between the high pressure and the cold denaturation mechanisms, despite the inherently different physical processes, and, directly related to it, the determinant role of hydration in protein stability.

Acknowledgements

We wish to thank Catherine Royer for helpful discussion and Stephen Martin for invaluable help with data interpretation.

References

Adinolfi, S., Trifuoggi, M., Politou, A., Martin, S., Pastore, A. (2002) A structural approach to understanding the iron-binding properties of phylogenetically different frataxins. Hum. Mol. Genet. 11, 1865-1877.

Adinolfi, S., Nair, M., Politou, A., Bayer, E., Martin, S., Temussi, P.A., Pastore, A. (2004) The factors governing the thermal stability of frataxin orthologues: how to increase a protein stability. Biochemistry 43, 6511-6518.

Adrover M, Esposito V, Martorell G, Pastore A, Temussi PA. (2010) Understanding cold denaturation: the case study of Yfh1. J Am Chem Soc. 132, 16240-6.

Adrover M, Martorell G, Martin SR, Urosev D, Konarev PV, Svergun DI, Daura X, Temussi P, Pastore A. (2012) The role of hydration in protein stability: comparison of the cold and heat unfolded states of Yfh1. J Mol Biol. 417, 413-24.

Bitonti A, Puglisi R, Meli M, Martin SR, Colombo G, Temussi PA, Pastore A. (2022) Recipes for Inducing Cold Denaturation in an Otherwise Stable Protein. J Am Chem Soc. 144, 7198-7207. doi: 10.1021/jacs.1c13355.

Castro IH, Pignataro MF, Sewell KE, Espeche LD, Herrera MG, Noguera ME, Dain L, Nadra AD, Aran M, Smal C, Gallo M, Santos J. (2019) Frataxin Structure and Function. Subcell Biochem. 93, 393-438.

Dellarole M, Caro JA, Roche J, Fossat J, Barthe P, Carcia-Moreno EB, Royer CA, Roumestand C. (2015) Evolutionarily Conserved Pattern of Interactions in a Protein Revealed by Local Thermal Expansion Properties. J Am Chem Soc. 137, 9354-62.

Dubois C, Herrada I, Barthe P, Roumestand C. (2020) Combining High-Pressure Perturbation with NMR Spectroscopy for a Structural and Dynamical Characterization of Protein Folding Pathways. Molecules. 25, 5551.

Dubois C, Planelles-Herrero VJ, Tillatte-Tripodi C, Delbecq S, Mammri L, Sirkia EM, Ropars V, Roumestand C, Barthe P. (2021) Pressure and Chemical Unfolding of an α-Helical Bundle Protein: The GH2 Domain of the Protein Adaptor GIPC1. Int J Mol Sci. 22, 3597.

Fossat MJ, Dao TP, Jenkins K, Dellarole M, Yang Y, McCallum SA, Garcia AE, Barrick D, Roumestand C, Royer CA. (2016) High-Resolution Mapping of a Repeat Protein Folding Free Energy Landscape. Biophys J. 111, 2368-2376.

Herrada I, Barthe P, Vanheusden M, DeGuillen K, Mammri L, Delbecq S, Rico F, Roumestand C. (2018) Monitoring Unfolding of Titin I27 Single and Bi Domain with High-Pressure NMR Spectroscopy. Biophys. J. 11, 341–352.

Jumper J, Evans R, Pritzel A, Green T, Figurnov M, Ronneberger O, et al. (2021) Highly accurate protein structure prediction with AlphaFold. Nature 596, 583–589.

Lahfa M, Mouhand A, de Guillen K, Barthe P, Kroj T, Padilla A, Roumestand C. (2023). Does a Similar 3D Structure Mean a Similar Folding Pathway? The Presence of a C-Terminal α-Helical Extension in the 3D Structure of MAX60 Drastically Changes the Folding Pathway Described for Other MAX-Effectors from Magnaporthe oryzae. Molecules 28, 6068.

Martin, S.R., Esposito, V., De Los Rios, P., Pastore, A., Temussi, P.A. Cold denaturation of yeast frataxin offers the clue to understand the effect of alcohols on protein stability. J Am Chem Soc. 2008 Jul 30;130(30):9963-70.

Musco G, Stier G, Kolmerer B, Adinolfi S, Martin S, Frenkiel T, Gibson T, Pastore A. (2000) Towards a structural understanding of Friedreich's ataxia: the solution structure of frataxin. Structure 8, 695-707.

Pastore A, Martin SR, Politou A, Kondapalli KC, Stemmler T, Temussi PA (2007) Unbiased cold denaturation: low- and high-temperature unfolding of yeast frataxin under physiological conditions. J Am Chem Soc.129, 5374-5.

Pastore, A., Temussi, P.A. (2022) The Protein Unfolded State: One, No One and One Hundred Thousand. J Am Chem Soc. 144, 22352-22357.

Pastore, A., Temussi, P.A. (2023) Unfolding under pressure: an NMR perspective. ChemBioChem. e202300164.

Piotto, M., Saudek, V., Sklenár, V. (1992). Gradient-tailored excitation for single-quantum NMR spectroscopy of aqueous solutions. J Biomol NMR 2, 661-5.

Pons JL, Malliavin TE, Delsuc MA. (1996). Gifa V. 4: A complete package for NMR data set processing. J Biomol NMR. 8, 445-52.

Popovic, M., Sanfelice, D., Pastore, C., Prischi, F., Temussi, P.A., Pastore, A. (2015) Selective observation of the disordered import signal of a globular protein by in-cell NMR: the example of frataxins. Protein Sci. 24, 996-1003.

Privalov P.L. (1990) Cold denaturation of proteins. Crit Rev Biochem Mol Biol. 25, 281-305.

Privalov, P.L. (1982) Stability of proteins. Proteins which do not present a single cooperative system. Adv. Protein Chem. 35 1 104.

Privalov, P.L. (1979) Stability of Proteins Small Globular Proteins. Advances in Protein Chemistry 33, 167-241.

Puglisi, R., Cioni, P., Gabellieri, E., Presciuttini, G., Pastore, A., Temussi P.A. (2022) Heat and cold denaturation of Yeast frataxin: the effect of pressure. Biophys J.; 121, 1502-1511.

Puglisi, R., Karunanithy, G., Hansen, D.F. *et al.* (2021) The anatomy of unfolding of Yfh1 is revealed by site-specific fold stability analysis measured by 2D NMR spectroscopy. Commun Chem 4, 127.

Puglisi R, Brylski O, Alfano C, Martin SR, Pastore A, Temussi PA. (2020) Quantifying the thermodynamics of protein unfolding using 2D NMR spectroscopy. Commun Chem 3**,** 100.

Roche J, Caro, JA, Norberto DR, Barthe P, Roumestand C, Schlessman JL, Garcia AE, Royer CA. (2012) Cavities determine the pressure unfolding of proteins. Proc. Natl. Acad. Sci. USA 109, 6945–6950.

Roche J, Caro JA, Dellarole M, Guca E, Royer CA, García-Moreno BE, Garcia AE, Roumestand C. (2013) Structural, energetic, and dynamic responses of the native state ensemble of staphylococcal nuclease to cavity-creating mutations. Proteins. 81, 1069-80.

Roche J, Royer CA, Roumestand C. (2017) Monitoring protein folding through high pressure NMR Spectroscopy. Prog. Nucl. Magn. Reson. Spectrosc. 102-103, 15-31.

Roche J, Royer CA. (2018) Lessons from pressure denaturation of proteins. J. R. Soc. Interface. 15, 20180244.

Roche J, Royer CA, Roumestand C. (2019) Exploring Protein Conformational Landscapes Using High-Pressure NMR. Methods Enzymol. 614:293-320.

Rouget JB, Schroer MA, Jeworrek C, Pühse M, Saldana JL, Bessin Y, Tolan M, Barrick D, Winter R, Royer CA. (2010) Unique features of the folding landscape of a repeat protein revealed by pressure perturbation. Biophys J. 98, 2712-21.

Sanfelice D, Puglisi R, Martin SR, Di Bari L, Pastore A, Temussi PA. (2014) Yeast frataxin is stabilized by low salt concentrations: cold denaturation disentangles ionic strength effects from specific interactions. PLoS One 9:e95801.

Sanfelice D, Morandi E, Pastore A, Niccolai N, Temussi PA. (2015) Cold Denaturation Unveiled: Molecular Mechanism of the Asymmetric Unfolding of Yeast Frataxin. Chemphyschem. 16, 3599-602.

Saotome T, Doret M, Kulkarni M, Yang YS, Barthe P, Kuroda Y, Roumestand C. (2019) Folding of the Ig-Like Domain of the Dengue Virus Envelope Protein Analyzed by High-Hydrostatic-Pressure NMR at a Residue-Level Resolution. Biomolecules 9, 309.

Smeller, L. (2002). Pressure-temperature phase diagrams of biomolecules. Biochimica et Biophysica Acta 1595, 11-29.

Söderberg CA, Shkumatov AV, Rajan S, Gakh O, Svergun DI, Isaya G, Al-Karadaghi S. (2011) Oligomerization propensity and flexibility of yeast frataxin studied by X-ray crystallography and small-angle X-ray scattering. J Mol Biol. 414, 783-97.

Vehlow C, Stehr H, Winkelmann M, Duarte JM, Petzold L, Dinse J, Lappe M. (2011) CMView: Interactive contact map visualization and analysis Bioinformatics 27, 1573–1574.

Vilanova, B., Sanfelice, D., Martorell, G., Temussi, P.A., Pastore, A. (2014) Trapping a salt-dependent unfolding intermediate of the marginally stable protein Yfh1. Frontiers in Molecular Biosciences 01/2014; 1.

Wishart DS, Bigam CG, Holm A, Hodges RS, Sykes BD. (1995) 1H, 13C and 15N random coil NMR chemical shifts of the common amino acids. I. Investigations of nearest-neighbor effects. J Biomol NMR. 5, 67-81.

Table 1 – Average residue-specific apparent free energy (<ΔG_u^0>) and volume (ΔV_u^0) of unfolding values measured at equilibrium and at atmospheric pressure and different temperatures. The values are compared to the equivalent ones obtained from fluorescence spectroscopy (Puglisi et al., 2022).

Temp (°C/K)	**<ΔG_u^0> (kcal/mol)**	**ΔV_u^0 (ml/mol)**	**<ΔG_u^0> (kcal/mol)**	**ΔV_u^0 (ml/mol)**
	Present study (NMR)		Puglisi et al., 2022 (Fluorescence)	

5/ 278	ND	ND	-0.20 ± 0.02	-87± 2
10/ 283	0.559 ± 0.212	-178 ± 19	-0.03 ± 0.02	-90 ± 4
15/ 288	0.649 ± 0.145	-165 ± 13	0.09 ± 0.05	-90 ± 2
20/ 293	0.472 ± 0.138	-149 ± 11	0.22 ± 0.07	-83 ± 3
25/ 298	0.409 ± 0.202	-134 ± 13	0.17 ± 0.02	-81 ± 2
30/ 303	0.089 ± 0.264	-130 ± 20	-0.08 ± 0.02	-70 ± 1
40/ 313	ND	ND	-0.19 ± 0.05	-59 ± 1

Figures

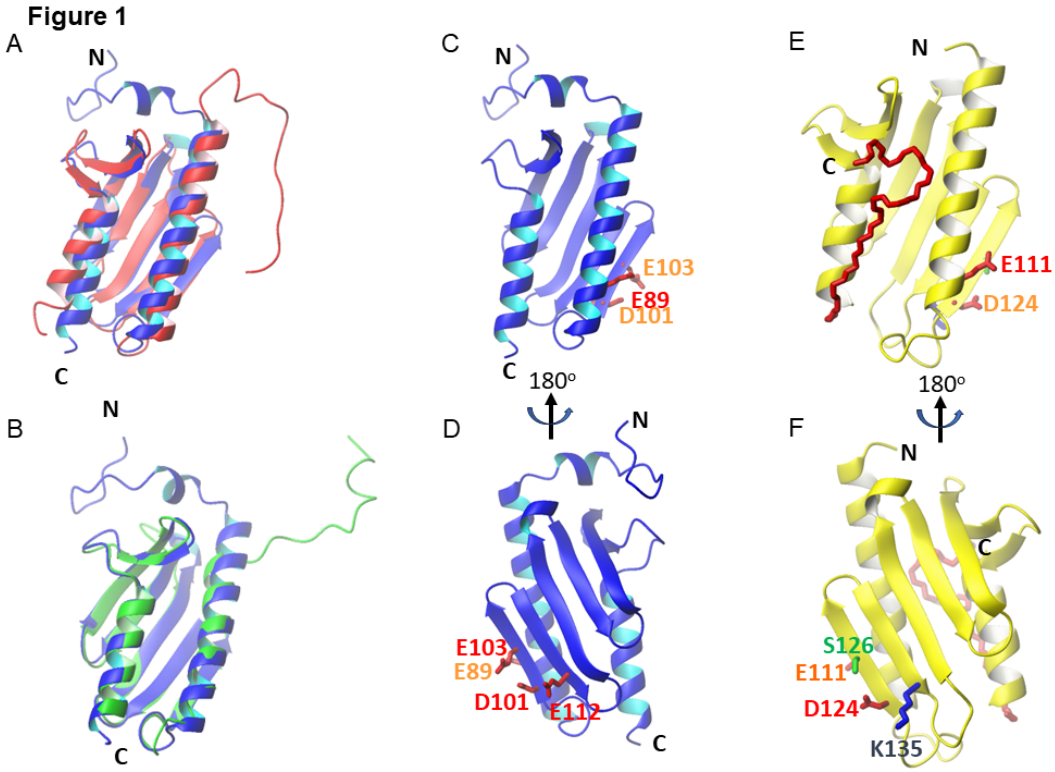

Figure 1 – Comparison between the experimental structures and the AlphaFold model of Yfh1. Superimposition of the 3D structures (ribbon representations) of the AlphaFold model of Yfh1 (blue ribbon) with **A**) the corresponding NMR solution structure (2ga5) and **B**) the X-ray structure (3eoq) (green ribbons). C) and D) Ribbon representation of the AlphaFold model of YFH1 in two different orientations differing by a 180° rotation around the y axis, highlighting the negatively charged patch that promotes electrostatic frustration and the C-short terminus. E) and F) For comparison the structure of human frataxin (1egk) on which the residues corresponding to the electrostatic patch are indicated and the much longer C-terminus that inserts in between the two helices and protects the hydrophobic core. The side chains of negatively charged residues are indicated in red, positive residues in blue and non-charged residues in green.

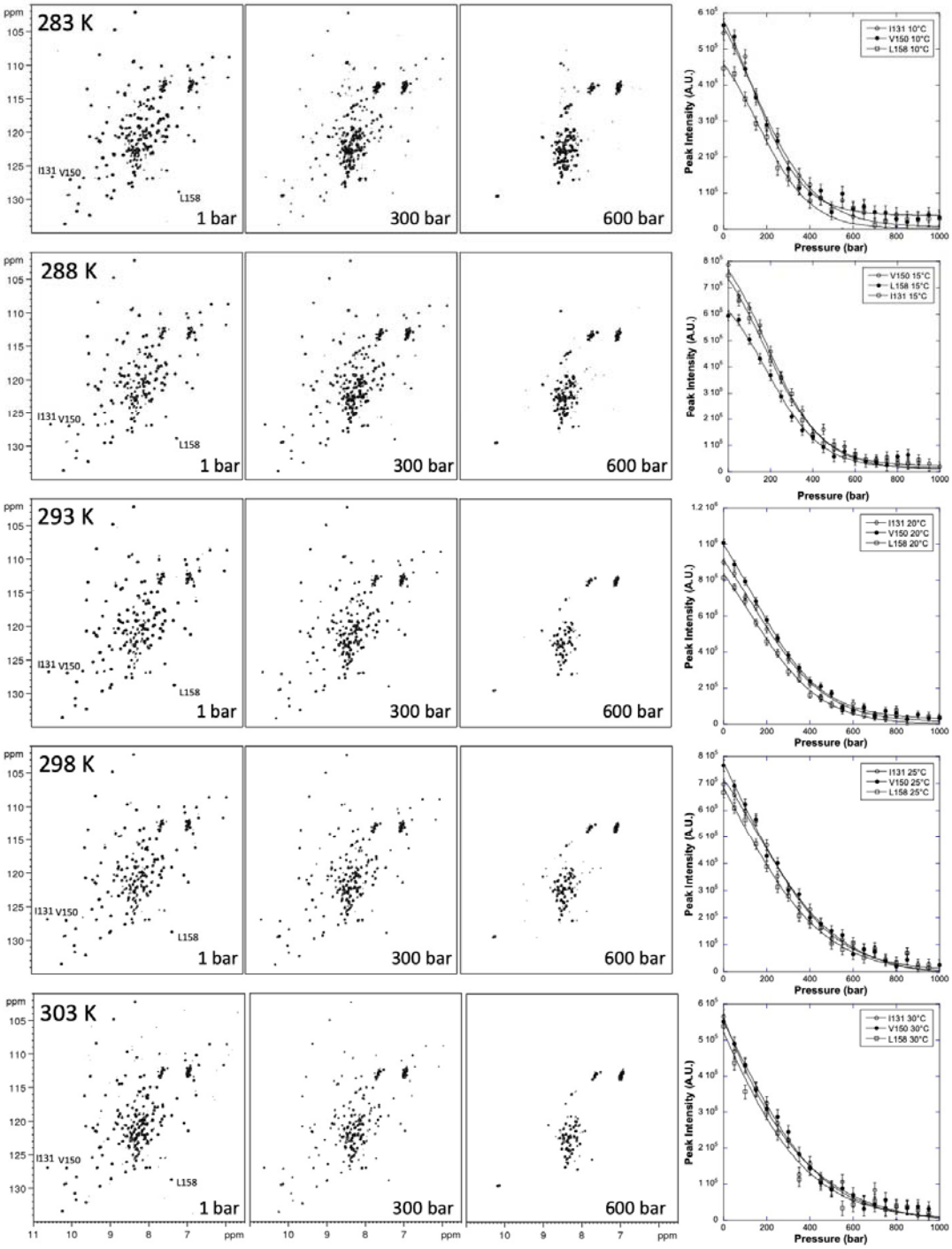

Figure 2. NMR monitored high-pressure unfolding of Yfh1. [^{1}H,^{15}N] HSQC spectra recorded at 283 K, 288 K, 293 K, 298 K and 303 K (from top to bottom, as indicated). At each temperature, spectra at 1, 300 and 600 bar are displayed from left to right. The rightmost panels report the overlays of residue-specific denaturation curves for three representative residues (I131, V150, and L1584, labelled on the corresponding HSQC at 1 bar) obtained from the fits of the pressure-dependent sigmoidal decrease of the corresponding residue cross-peak intensities in the HSQC spectra with Eq. 1.

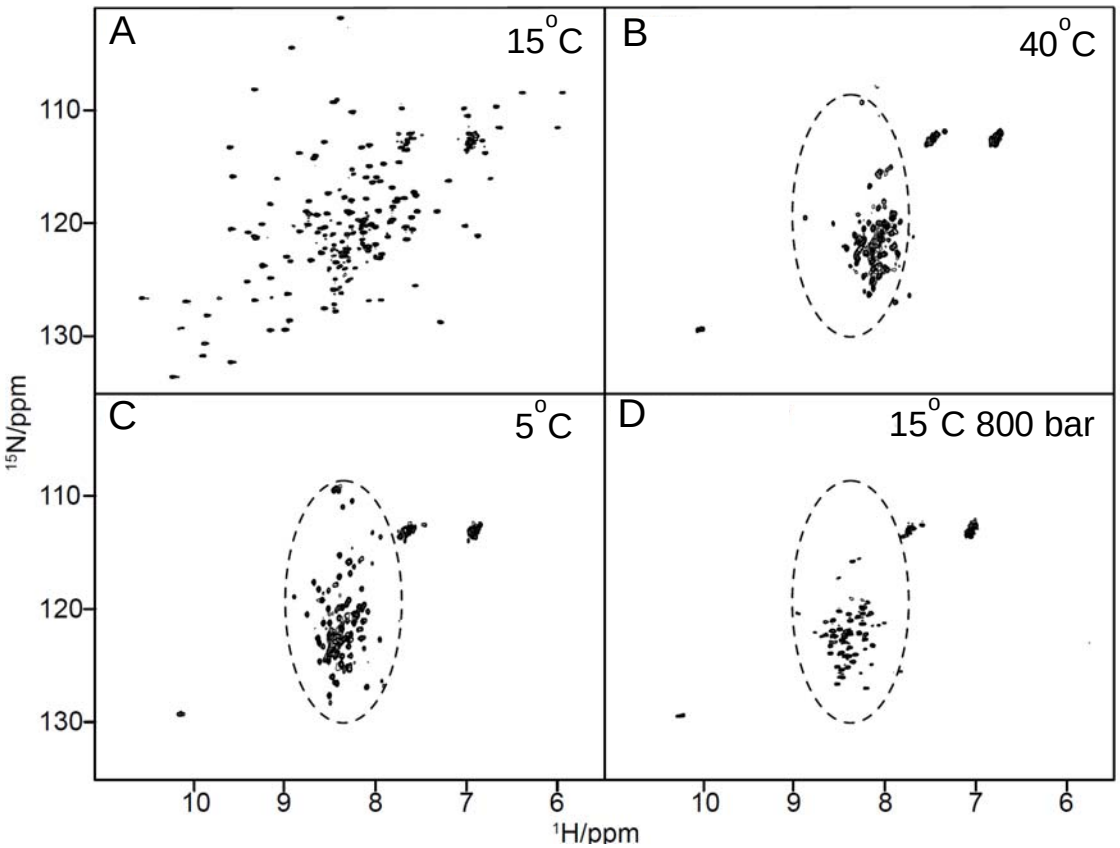

Figure 3. Comparison of the HSQC spectra of Yfh1 under different conditions. A) Spectrum recorded at the temperature of maximal stability of the protein and room pressure. The spectrum has excellent dispersion and all the features typical of a folded protein. B) Unfolded spectrum at 313 K and room pressure. C) Unfolded spectrum at 278 K and room pressure. D) Unfolded spectrum at 288 K and 800 bar. A dotted oval is drawn in the same region of the various unfolded spectra which roughly corresponds to the area span by all peaks in the cold denatured spectrum. The three spectra show a similar collapse of the resonance dispersion, but the heat denatured is noticeably up-shifted as compared to the cold denatured spectrum as previously analysed (Adrover et al., 2010 and 2012). This indicates a different level of hydration that is higher at low temperature. The pressure-denatured spectrum has overall features closer to the cold denatured one.

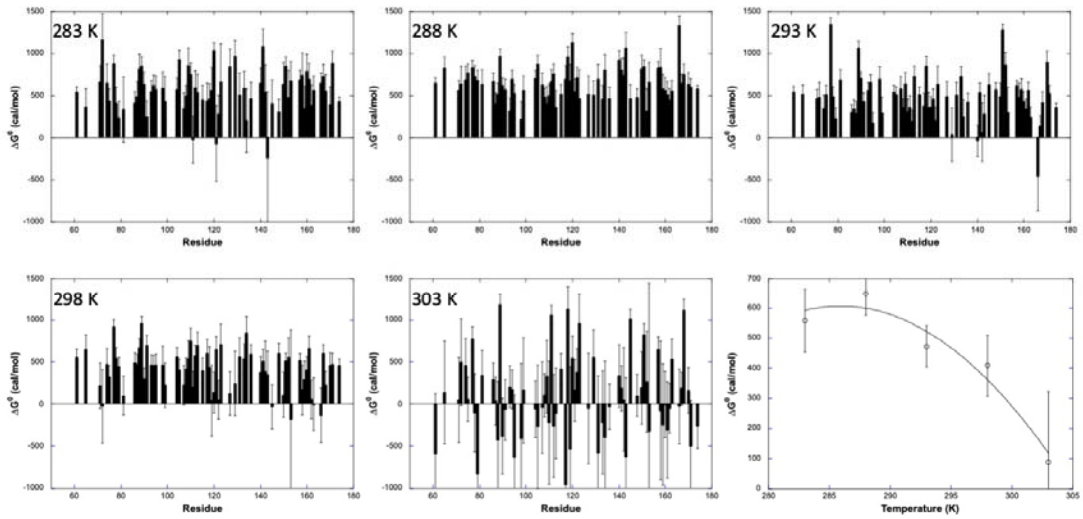

Figure 4. Apparent Residue-Specific difference of Gibbs Free Energy of Unfolding (ΔG_u^0) values measured for Yfh1 at 283 K, 288 K, 293 K, 298 K and 303 K (as indicated) from residue-specific pressure denaturation curves. The residue numbering used in the figure corresponds to the one deposited for the X-ray structure (3EOQ). The last panel displays the averaged values of ΔG_u^0 at each temperature versus the temperature, fitted with the Gibbs-Helmotz equation (Eq. 2).

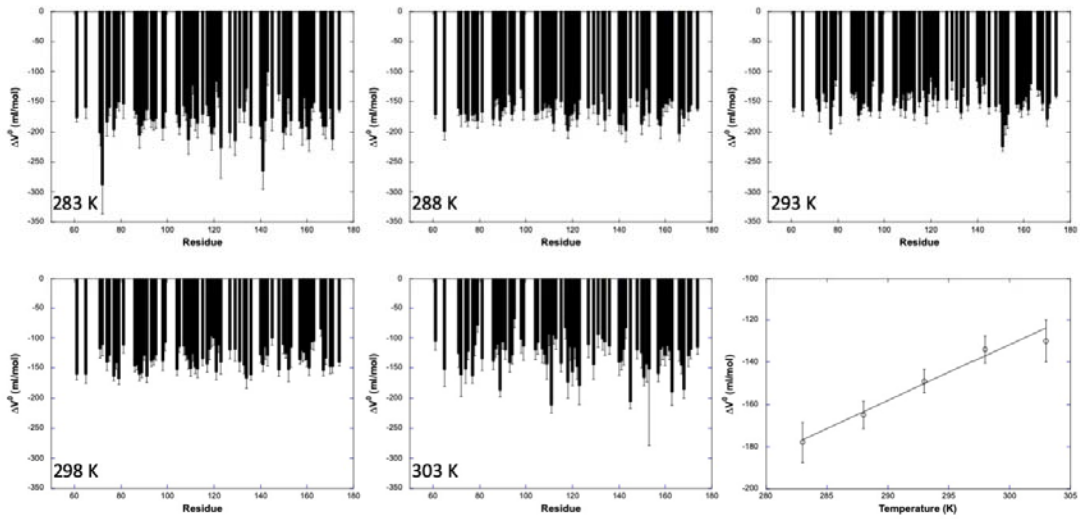

Figure 5. Apparent Residue-Specific Volume Change of Unfolding (ΔV_u^0) values measured for Yfh1 at 283 K, 288 K, 293 K, 298 K and 303 K (as indicated) from residue-specific pressure denaturation curves. The residue numbering used in the figure corresponds to the one deposited for the X-ray structure (3EOQ). The last panel displays the linear fit of the averaged values of ΔV_u^0 at each temperature versus the temperature.

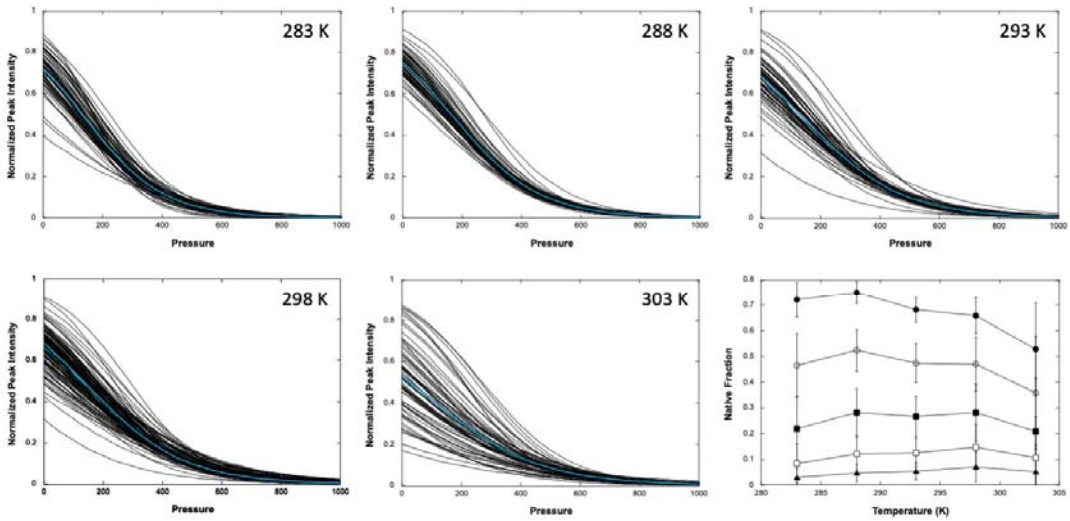

Figure 6. Normalized residue-specific denaturation curves at different temperatures. The bold cyan curves represent the average normalized curve at each temperature. The last panel display the evolution of the native fraction of the protein (obtained from the average normalized curves) as a function of the temperature at 1 (filled circles), 150 (open circles), 300 (filled squares), 450 (open squares) and 600 bar (filled triangles).

A

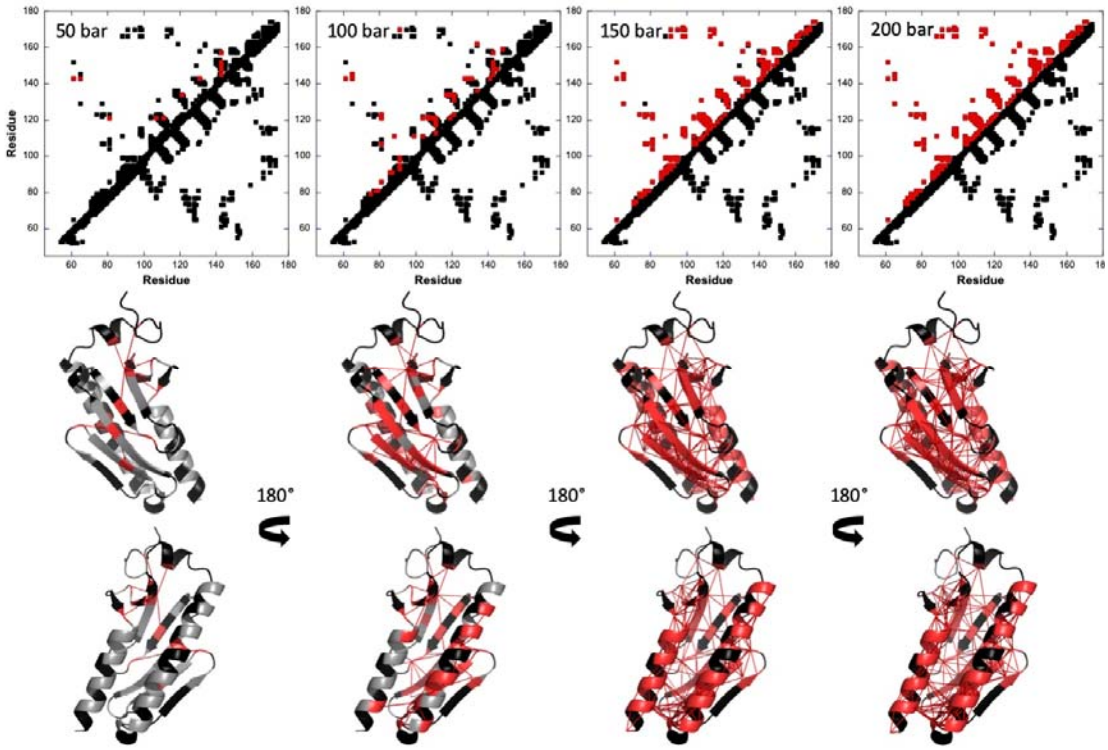
50 bar
100 bar
150 bar
200 bar
Residue
Residue
180°
180°
180°

B

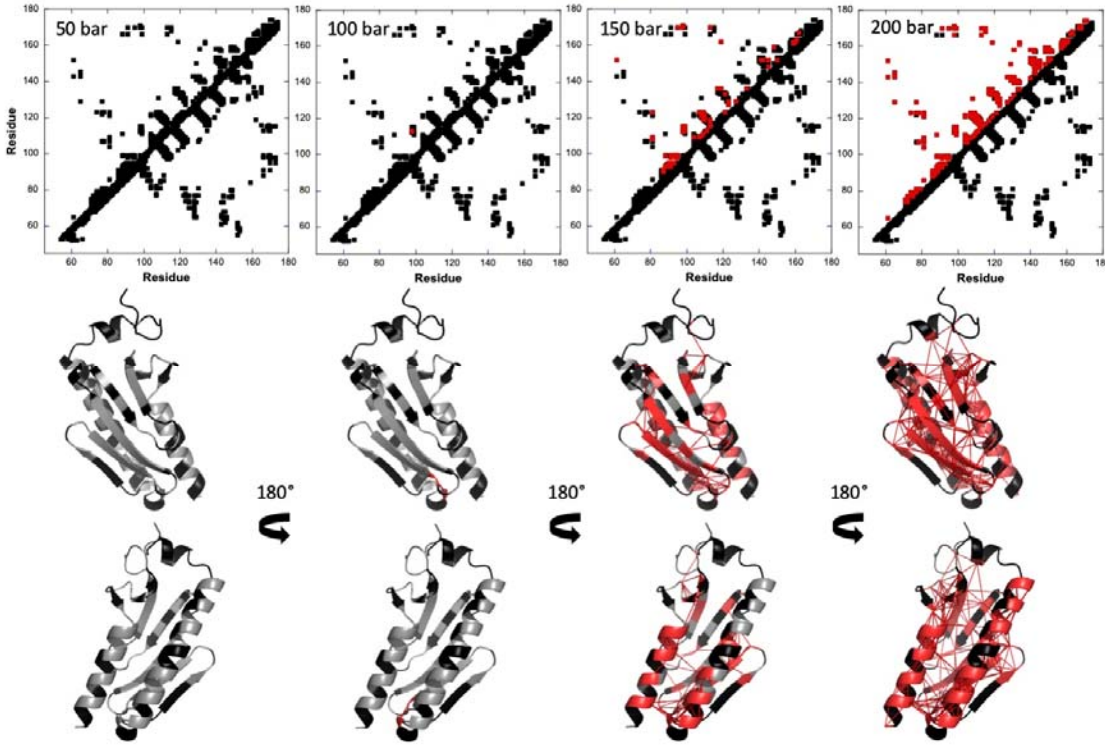
50 bar
100 bar
150 bar
200 bar
Residue
Residue
180°
180°
180°

C

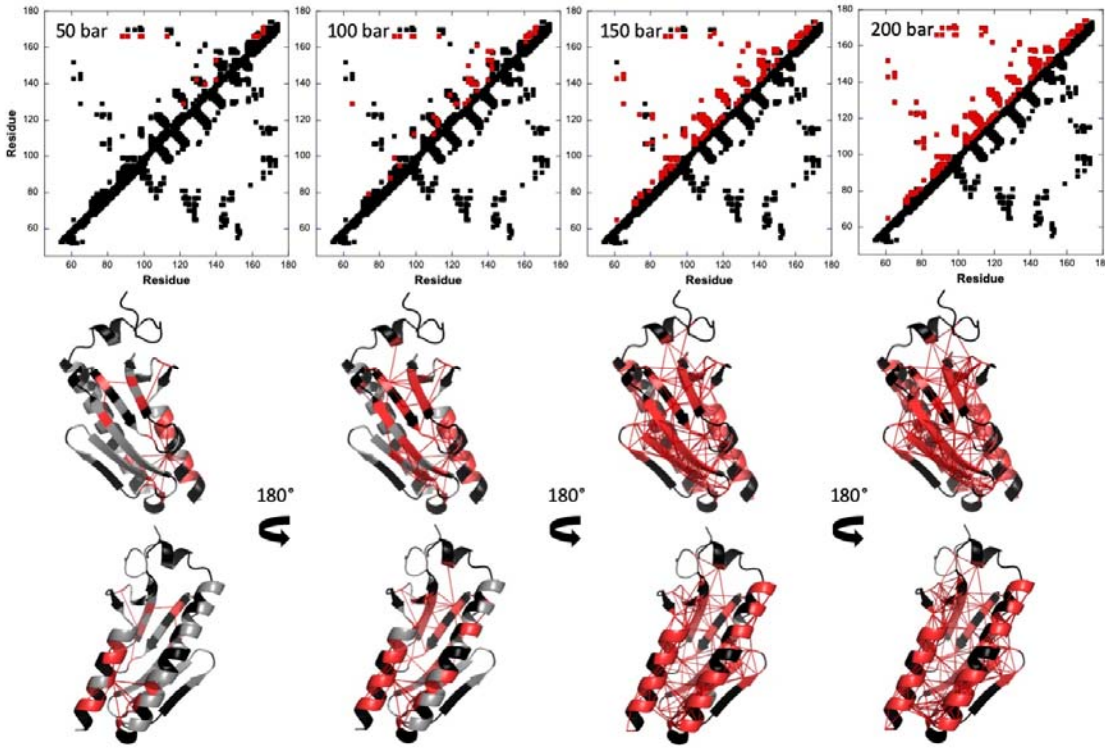
50 bar
100 bar
150 bar
200 bar
Residue
Residue
180°
180°
180°

D

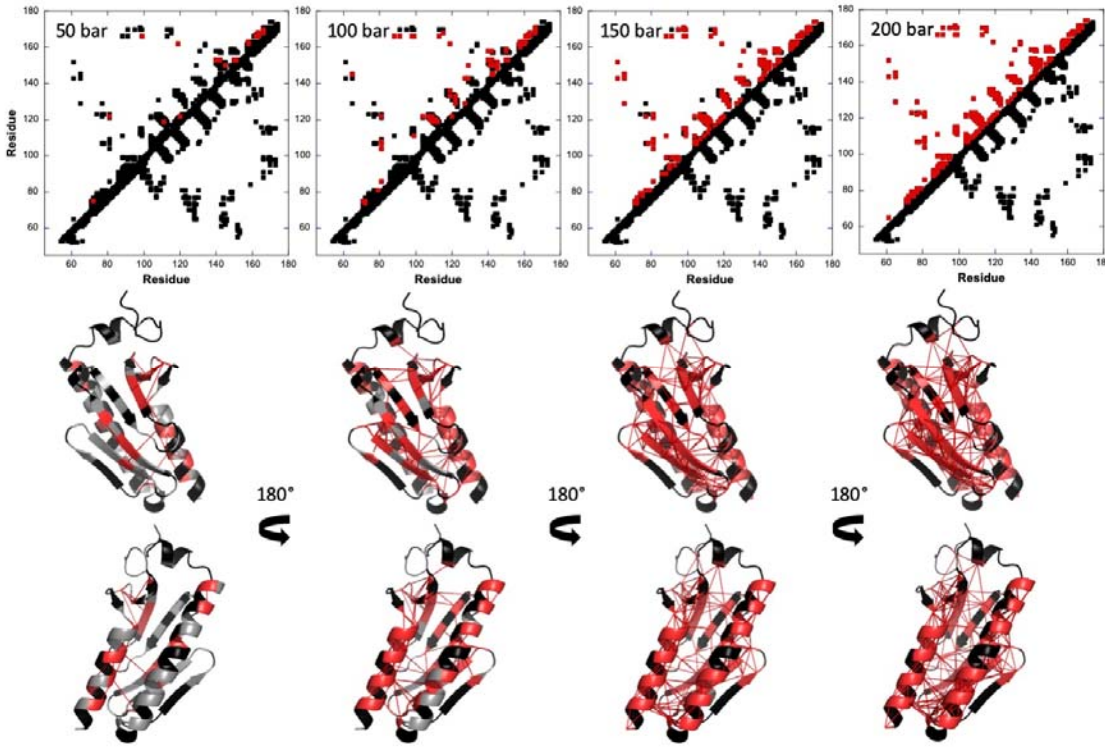
50 bar
100 bar
150 bar
200 bar
Residue
Residue
180°
180°
180°

E

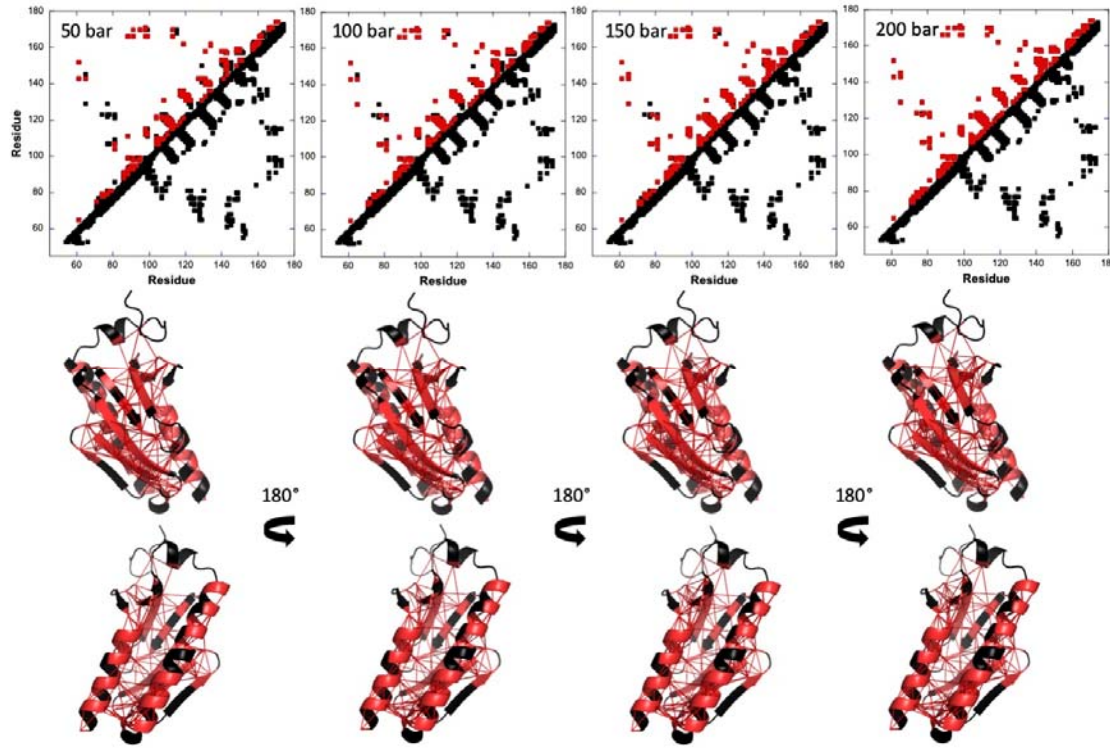

Figure 7. The pathway of pressure denaturation of Yfh1 at different temperatures and pressure. Data collected at (A) 283 K, (B) 288 K, (C) 293 K, (D) 298 K and (E) 303 K. Top) Fractional contact maps built from the AlphaFold model at 50, 100, 150 and 200 bar, as indicated. Contacts below the diagonal were calculated with CMview and correspond to residues where the distance between corresponding Cα atoms is lower than 9.5 Å. Above the diagonal, only the contacts (> i, i+1) for which fractional probability can be obtained have been reported. In addition, residues have been colored in red when contact probabilities P_{ij} lower than 0.5 are observed. Bottom**)** Visualization of the probabilities of contact on ribbon representations of Yfh1 (opposite views that differ for a 180° rotation along the vertical axis) at 50, 100, 150 and 200 bar. The red lines represent contacts that are significantly weakened (P_{ij} < 0.5) at the corresponding pressure. Residues involved in these contacts are colored in red, and residues for which fractional probability cannot be obtained are colored in black.